

## Article

# Electronic, Elastic, and Thermoelectric Properties of Half-Heusler Topological Semi-Metal HfIrAs from First-Principles Calculations

Muyiwa Kehinde Bamgbose <sup>1,\*</sup>, Funmilayo Ayedun <sup>2</sup>, Gbenro Timothy Solola <sup>3</sup> , Abolore Adebayo Musari <sup>4</sup>,  
Stephane Kenmoe <sup>5,\*</sup> and Gboyega Augustine Adebayo <sup>6,\*</sup> 

<sup>1</sup> Department of Physics, Lagos State University, Ojo 102101, Nigeria

<sup>2</sup> Department of Physics, National Open University of Nigeria, Abuja 106104, Nigeria

<sup>3</sup> Department of Physics, Augustine University Ilara-Epe, Epe 106103, Nigeria

<sup>4</sup> Physics with Electronics Unit, Department of Science Laboratory Technology, Moshood Abiola Polytechnic, Abeokuta 110104, Nigeria

<sup>5</sup> Department of Theoretical Chemistry, University of Duisburg-Essen, Universitätsstr. 2, D-45141 Essen, Germany

<sup>6</sup> Department of Physics, Federal University of Agriculture, Abeokuta 111101, Nigeria

\* Correspondence: muyiwa.bamgbose@lasu.edu.ng (M.K.B.); stephane.kenmoe@uni-due.de (S.K.); adebayo@physics.unaab.edu.ng (G.A.A.)

**Abstract:** The ab initio method is used to calculate the electronic, elastic, lattice-dynamic, and thermoelectric properties of the semimetal Half-Heusler compound HfIrAs. Density Functional Theory within Generalized Gradient Approximation is used to carry out calculations of lattice parameters, band structure, electronic density of states, phonon band structure, phonon density of states, elastic moduli, specific heat at constant volume, the Seebeck coefficient, electrical conductivity, the power factor, and the dimensionless figure of merit. The electronic band structure reveals that the compound is semimetal. The phonon dispersion shows that HfIrAs is dynamically stable. The projected phonon density of states, which shows the contribution of each constituent atom at every frequency level, is also reported. The ratio of bulk modulus to shear modulus is 2.89; i.e., the material is ductile, and it satisfies stability criteria. The thermoelectric properties of this compound at different temperatures of 300 K, 600 K, and 800 K are reported as a function of hole concentration for the first time to the best of our knowledge. The dimensionless figure of merit of HfIrAs is 0.57 at 800 K when the doping concentration is  $0.01 \times 10^{20} \text{ cm}^{-3}$ . Therefore, this compound is predicted to be a good thermoelectric material.

**Keywords:** first-principles; elastic; thermoelectric; electronic; phonon; compounds



**Citation:** Bamgbose, M.K.; Ayedun, F.; Solola, G.T.; Musari, A.A.; Kenmoe, S.; Adebayo, G.A. Electronic, Elastic, and Thermoelectric Properties of Half-Heusler Topological Semi-Metal HfIrAs from First-Principles Calculations. *Crystals* **2023**, *13*, 37. <https://doi.org/10.3390/cryst13010037>

Academic Editor: Andrei Vladimirovich Shevelkov

Received: 21 November 2022

Revised: 20 December 2022

Accepted: 22 December 2022

Published: 26 December 2022



**Copyright:** © 2022 by the authors. Licensee MDPI, Basel, Switzerland. This article is an open access article distributed under the terms and conditions of the Creative Commons Attribution (CC BY) license (<https://creativecommons.org/licenses/by/4.0/>).

## 1. Introduction

First-principle Density Functional Theory (DFT) has been widely used to predict the properties of materials [1–4]. The properties predicted by DFT cut across many fields, which include Materials Science, Computational Chemistry, Condensed Matter Physics, Engineering, Solid Earth Physics, and other areas of materials science. The DFT probe of materials can reveal the intrinsic properties of the materials. It can be employed to obtain materials' desirable properties for specific applications. The accuracy of DFT as a computational tool is excellent, as it introduces more approximations into the Kohn–Sham equations to solve various categories of material systems of materials [5–8]. DFT is increasingly employed to determine the properties of materials for energy harvesting and conversion.

The HfIrAs half-Heusler compound has been extensively studied theoretically in many works of literature; for instance, its optoelectronic properties and thermoelectric performance as a function of carrier concentration and chemical potentials were reported

by Chibani et al. [9]. The spin–orbit coupling effect on the structural, electronic, and optical properties of the HfIrAs half-Heusler compound, in addition to theoretical estimation of some of its other physical properties, were reported by Gautier et al. [10]. Wang and Wei [11] studied topological phases changes and atom substitutions in the HfIrAs half-Heusler compound and predicted the HfIrAs compound as a nontrivially topological semi-metal. Arikan et al. [12] presented the electronic, elastic, vibrational, and thermodynamic properties and the effect of spin–orbit coupling on the HfIrAs half-Heusler compound. The present work majorly addressed the thermoelectric properties of p-type HfIrAs at different temperature as a function of holes concentration, which is scarce in most studies to the best of our knowledge. The elastic and dynamical properties of HfIrAs were also computed to affirm its mechanical and dynamical stability, while the electronic and optical properties were calculated to compare them with other theoretical observations.

The half-Heusler (HH) compounds are among the most widely studied compounds both theoretically and experimentally because of their potential applications in thermoelectrics and spintronics [13–16]. This is by the virtue of their remarkable and exceptional properties, such as their high Seebeck coefficient, low thermal conductivity, high thermal stability, high electrical conductivity, high power factor, high figure of merit, and high electronic fitness function [17–19]. The exciting properties of HH compounds have gained the attention of materials physics researchers, who are now expanding their search for materials with a high figure of merit, high electronic fitness function, and high thermal stability. The attention given to HH compounds is tremendous and perpetual because of global demands for maximum energy from fossil fuels. The waste of a large portion of fossil energy is in the form of heat. The waste heat from fossil fuels causes a rise in temperature, which results in global warming and its accompanying adverse effects on living and non-living things. According to Bian, converting waste heat into energy will increase the energy output from fossil fuels while also reducing global warming [20].

HH compounds have a general chemical formula, XYZ, where X and Y are transition metals and Z is the main group element. HH compounds crystallize in the  $C1_b$  Face Centre Cubic (FCC) structure; the space group of HH is  $F\bar{4}3m$ , space group number 216. Three atoms occupy the face-centered cubics (FCC) positions X, Y, and Z, while one Y position is empty. The most electropositive transition metal will occupy Wyckoff's position 0.25 0.25 0.25. In HH compounds, the atoms on Wyckoff positions 4a (0, 0, 0) and 4b (0.5, 0.5, 0.5) form the ionic NaCl-type substructure, and the atoms on 4a and 4c build the covalent ZnS-type substructure [21–24]. HH compounds with valence electron counts (VEC) of 8 and 18 electrons are semiconductors and semimetals, respectively [11,25–33]. HH compounds with 8 or 18 VEC are high-performance thermoelectric materials with stable structures in the temperature range of 0–1000 K. In recent times, tremendous simulation work on energy production has focused on the properties of HH compounds. The work on HH is due to its simple structure and applications in piezoelectrics, optoelectronics, magnetism, solar cells, half-metallicity, superconductivity, and thermoelectricity [16,34–39].

Human activities wholly depend on energy and the world's energy supply depends on fossil fuels. The burning of fossil fuel is not environmentally friendly and contributes in no small measure to global warming. Given this, there is a need to search for an alternate energy source. This search can be achieved by converting waste heat from burning fuel to electricity and converting geothermal energy to electricity. For decades, the attention of material scientists has shifted to the study of HH compounds. HH compounds are studied because of their ability to convert heat to electricity, and these compounds can be harnessed to serve as an alternative energy source by converting heat into electricity [40–66]. Based on the ability of HH compounds to convert heat to electricity, materials scientists focus on calculations of the properties of these compounds to discover more high-performance thermoelectric materials.

## 2. Computational Details

The FCC structure of HfIrAs (Figure 1) is simulated using DFT [42–46] within the Generalized Gradient Approximation to the Exchange Correlation (XC) Functional [47–49], with the Perdew–Burke–Ernzerhof (PBE) parameterization favor for solids (PBEsol) (Perdew) as implemented in the quantum ESPRESSO package [51–53]. The optimized energy cutoff of 60 Ry is used in this calculation to expand the plane wave. The convergence thresholds on total energy (a.u) and forces are  $10^{-4}$  Ry and  $10^{-3}$  Ry/au, respectively. Brillouin zone (BZ) integration was carried out by using the tetrahedron method over a special k-points mesh of  $10 \times 10 \times 10$  using the standard technique of Monkhorst and Pack [54]. The atomic arrangement of HfIrAs on Wyckoff's positions is as follows: Hf is located at (0.50, 0.50, 0.50), Ir is located at (0.25, 0.25, 0.25), As is located at (0.00, 0.00, 0.00), and the position (0.75, 0.75, 0.75) is vacant.

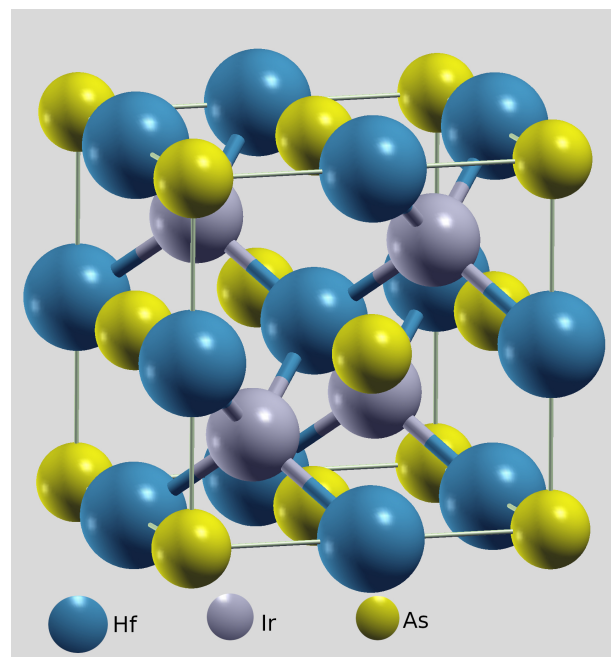


**Figure 1.** Crystal Structure of HfIrAs half-Heusler compound.

The system geometry was relaxed using the Broyden–Fletcher–Goldfarb–Shanno (BFGS) algorithm, and various values of lattice parameters were minimized with respect to the ground-state total energy of the system to obtain the optimized equilibrium lattice parameter. Phonon dispersion was obtained from the dynamic matrix at q-points of  $4 \times 4 \times 4$  grid in the first BZ. The thermoelectric properties of this compound were obtained by solving the semi-classical Boltzmann transport equation with a constant relaxation approximation as implemented in the BoltzTraP code [55,56]. Semi-classical Boltzmann theory equations were solved to obtain energy (E), carrier concentration (n), temperature (T), Seebeck's coefficient (S), electrical conductivity ( $\sigma$ ), thermal conductivity (k), power factor (PF), and a dimensionless figure of merit (zT) according to the following equations [57]:

$$S_{\alpha\beta}(T, \mu) = \frac{1}{eT\Omega\sigma_{\alpha\beta}(T, \mu)} \int \bar{\sigma}_{\alpha\beta}(\varepsilon)(\varepsilon - \mu) \left[ \frac{\partial f_0(T, \varepsilon, \mu)}{\partial \varepsilon} \right] d\varepsilon \quad (1)$$

$$\sigma_{\alpha\beta}(T, \mu) = \frac{1}{\Omega} \int \bar{\sigma}_{\alpha\beta}(\varepsilon) \left[ - \frac{\partial f_0(T, \varepsilon, \mu)}{\partial \varepsilon} \right] d\varepsilon \quad (2)$$

$$K_{\alpha\beta}^o(T, \mu) = \frac{1}{e^2 T \Omega} \int \bar{\sigma}_{\alpha\beta}(\varepsilon)(\varepsilon - \mu)^2 \left[ - \frac{\partial f_0(T, \varepsilon, \mu)}{\partial \varepsilon} \right] d\varepsilon \quad (3)$$

The transport distribution function  $\bar{\sigma}_{\alpha\beta}$  that appears in Equations (1)–(3) is defined as

$$\bar{\sigma}_{\alpha\beta}(\varepsilon) = \frac{e^2}{N} \sum_{i,k} \tau_i V_{\alpha}(i, \vec{k}) \cdot V_{\beta}(i, \vec{k}) \cdot \frac{\delta(\varepsilon - \varepsilon_{i, \vec{k}})}{d\varepsilon} \quad (4)$$

$$PF = S^2\sigma \quad (5)$$

$$zT = (S^2\sigma/k)T \quad (6)$$

The moduli of elasticity of this compound are obtained by calculating the Bulk modulus (B), Shear modulus (G), Young modulus (E), Poisson's ratio, and anisotropic factor (A) [58–63]

$$B = \frac{(c_{11} + 2c_{13})}{3} \quad (7)$$

$$G_v = \frac{(c_{11} - c_{12} + 3c_{44})}{5} \quad (8)$$

$$G_R = \frac{5c_{44}(c_{11} - c_{12})}{4c_{44} + 3(c_{11} - c_{12})} \quad (9)$$

$$G = \frac{G_v + G_R}{2} \quad (10)$$

$$E = \frac{9BG}{3B + G} \quad (11)$$

$$\nu = \frac{(3B - 2G)}{2(3B + G)} \quad (12)$$

$$A = \frac{2c_{44}}{c_{11} - c_{12}} \quad (13)$$

$$a = 1, \quad (14)$$

### 3. Results and Discussion

#### 3.1. Lattice Constant of HfIrAs

The ground-state total energy of the magnetic and non-magnetic phases of HfIrAs was calculated. The ground state total energy obtained for the two phases is given in Table 1. The result obtained for total energy minimization with respect to the phases show that the non-magnetic phase is energetically favored to be more stable; therefore, HfIrAs is a non-magnetic semi-metal HH compound. The HfIrAs structure is optimized using converged energy cutoff and k-point values. The optimized lattice parameter used for this work was obtained by calculating the total energy at different values of lattice parameters chosen around the lattice parameters from the studies [11,25–33]. Furthermore, the total energy–lattice parameters relationship was fitted to the Birch–Murnaghan third-order equation of state to obtain the equilibrium lattice constant. The obtained equilibrium lattice constant of HfIrAs is 6.07 Å, and this value is in very good agreement with the previously obtained value of the HfIrAs equilibrium lattice constant [11,12].

**Table 1.** Table of magnetic phases of HfIrAs.

Compounds	Phase	Total Energy
HfIrAs	Non-Magnetic	−380.37197933
HfIrAs	Magnetic	−380.37195502

#### 3.2. Elastic Properties of HfIrAs

There are three independent elastic constants in the cubic system:  $c_{11}$ ,  $c_{12}$ , and  $c_{44}$ . The stability criteria are  $c_{11} > 0$ ,  $c_{44} > 0$ ,  $c_{12} > B > c_{11}$ ,  $c_{11} - c_{12} > 0$ , and  $c_{11} + 2c_{12} > 0$  [64–67]; the compound is mechanically stable. The three independent elastic constants obtained

in this work are given in Table 2. The bulk modulus, shear modulus, Young's modulus, ratio of bulk modulus to shear modulus, Zener anisotropy factor, and Poisson's ratio are also given in Table 2. The bulk modulus of HfIrAs obtained is 176.71 GPa, which is higher than the bulk moduli of steel and aluminium [68]. This shows that HfIrAs is mechanically strong. The ductility or brittleness of materials can be determined based on Pugh's scale [69]; on this scale, materials with  $B/G > 1.75$  are ductile. The  $B/G$  value of HfIrAs in this work is 2.89; this shows that HfIrAs is ductile. Table 2 shows that HfIrAs is an anisotropic compound. The shear modulus of HfIrAs is 61.14 GPa; this is the measure of the resistance of HfIrAs to shear deformation. The dynamical stability of materials is determined by the condition  $c_{11} - c_{12} > 0$ ; HfIrAs meets this condition, so we can conclude that it is dynamically stable. The Poisson's ratio of the material is 0.34; this is the measure of the plasticity of this material. According to Rogl, the Poisson's ratio of this material is relatively high when compared to that of other half-Heusler compounds. The elastic constants obtained in this work are in good agreement with those in previous work [12].

**Table 2.** Table of elastic constant of HfIrAs.

Elastic Constants	HfIrAs	Ref [12]
$c_{11}$ (GPa)	240.92	222.42
$c_{12}$ (GPa)	144.60	129.84
$c_{44}$ (GPa)	71.71	94.20
$B$ (GPa)	176.71	156.20
$G$ (GPa)	61.14	70.83
$E$ (GPa)	164.44	185.26
$B/G$	2.89	2.27
$n$	0.34	0.31
$A$	1.49	2.03

### 3.3. Band Structure of HfIrAs

The electronic band structure and electronic Density of States (DOS) of HfIrAs are shown in Figure 2a. In this band structure, a pair of bands touch at the gamma ( $\Gamma$ ) point in the momentum space. Materials that have this feature of touching pairs of bands are semimetals. Semi-metal Heusler compounds behave like semiconductors and are materials of interest in energy generation [70,71]. The semimetal HfIrAs half-Heusler compound has a parabolic band that improves conductivity as well as a flat band in the K-space between ( $\Gamma$ ) and  $L$  points. The flat bands enhance the Seebeck coefficient, thereby making materials better thermoelectric candidates. According to the DOS, the d-orbital of the  $Hf$  atom dominates the conduction band of HfIrAs, while the d-orbital of the  $Ir$  atom contributes significantly to the valence band.

### 3.4. Lattice Dynamics and Thermodynamic Properties of HfIrAs

The lattice dynamic and thermoelectric properties of HfIrAs were obtained from Density Functional Perturbation Theory (DFPT) within harmonic approximation (QHA). The phonon band structure of HfIrAs is shown in Figure 2b. The three atoms in this compound result in four transverse optical (TO) modes, two longitudinal optical (LO) modes, two transverse acoustic (TA) modes, and one longitudinal acoustic (LA) mode. The phonon band structure has nine branches in total. This is an expected property of compounds with three atoms per unit cell, as well as a property of half-Heusler compounds [32,72]. According to the phonons DOS in Figure 2b, the As atom dominates the optical mode in the frequency range of 175–210  $\text{cm}^{-1}$ . In the acoustic mode, the highest contribution comes from the Ir atom. There is a frequency band gap between the optical mode and acoustic mode, and the frequency band gap reduces thermal conductivity. The absence of negative frequencies in the band structure confirms that the compound HfIrAs is dynamically stable. The gap between the frequencies of acoustic and optical modes is a function of differences in the

masses of the atoms that make up the compounds. The masses' difference is directly proportional to the gap in the frequencies.

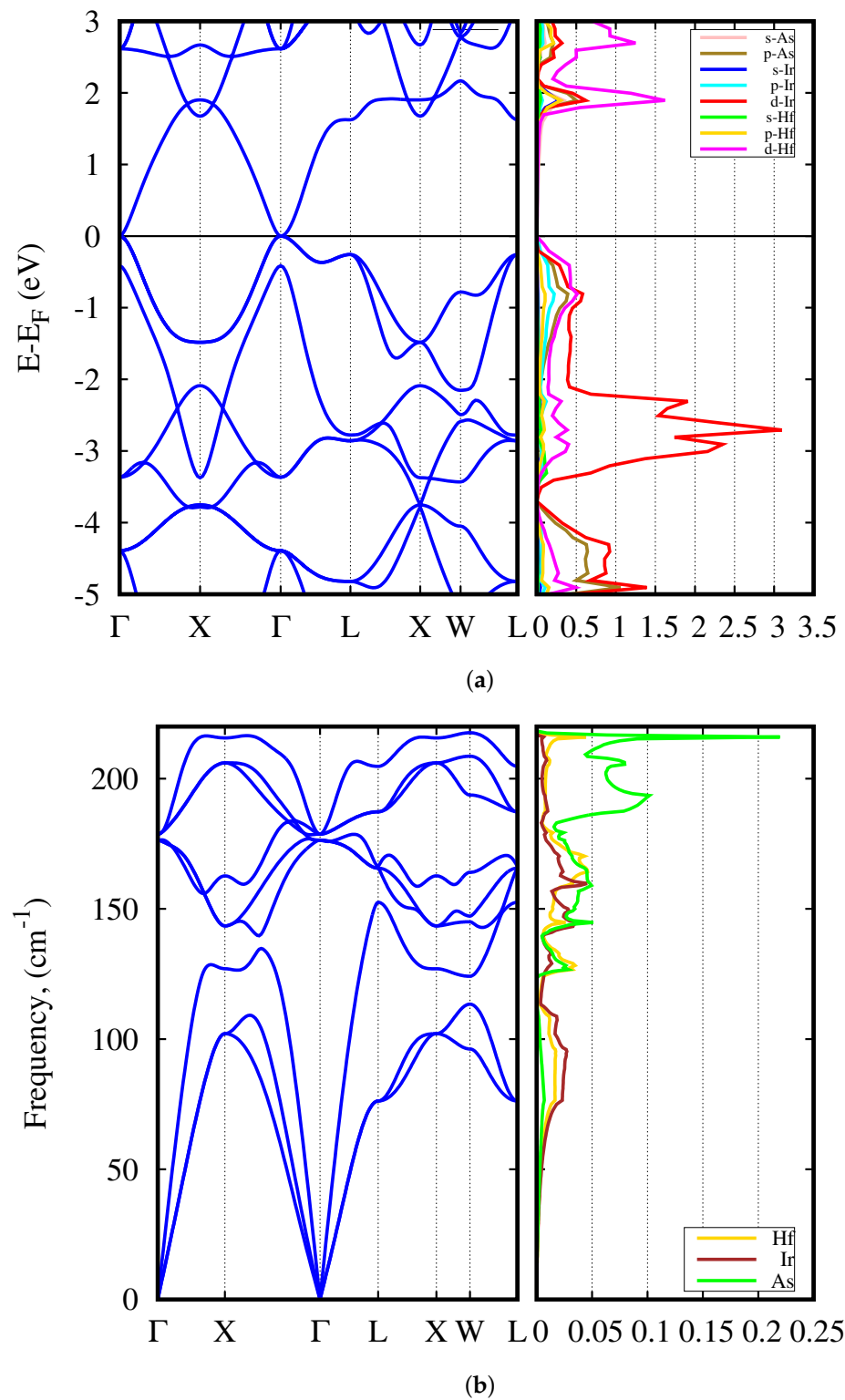


**Figure 2.** (a) Electronic band structure and corresponding partial density of state, and (b) phonon band structure and projected phonon density of state for HfIrAs half-Heusler compound.

The thermodynamic properties are obtained from the quasi-harmonic Debye model [73–75]. Figure 3 depicts the entropy, internal energy, heat capacity, and vibrational

free energy as a function of temperature. The thermodynamic properties of HfIrAs reveal the behaviour of this material under various temperatures, and information about this behaviour is mostly obtained from the heat capacity curve. The heat capacity at constant volume of HfIrAs in the temperature range of 0–1200 K is displayed in Figure 3. The heat capacity at constant volume ( $C_v$ ) increases with temperature on its own. The  $C_v$  becomes fairly constant at a temperature above 300 K. At this temperature, the thermal energy excites all the phonons. The coefficient of vaporization  $C_v$  of this material becomes constant at temperatures above 400 K; at constant  $C_v$ , the material obeys Dulong–Petit’s law [76] at a temperature of around 600 K and a  $C_v$  of  $74 \text{ Jmol}^{-1}\text{K}^{-1}$ .

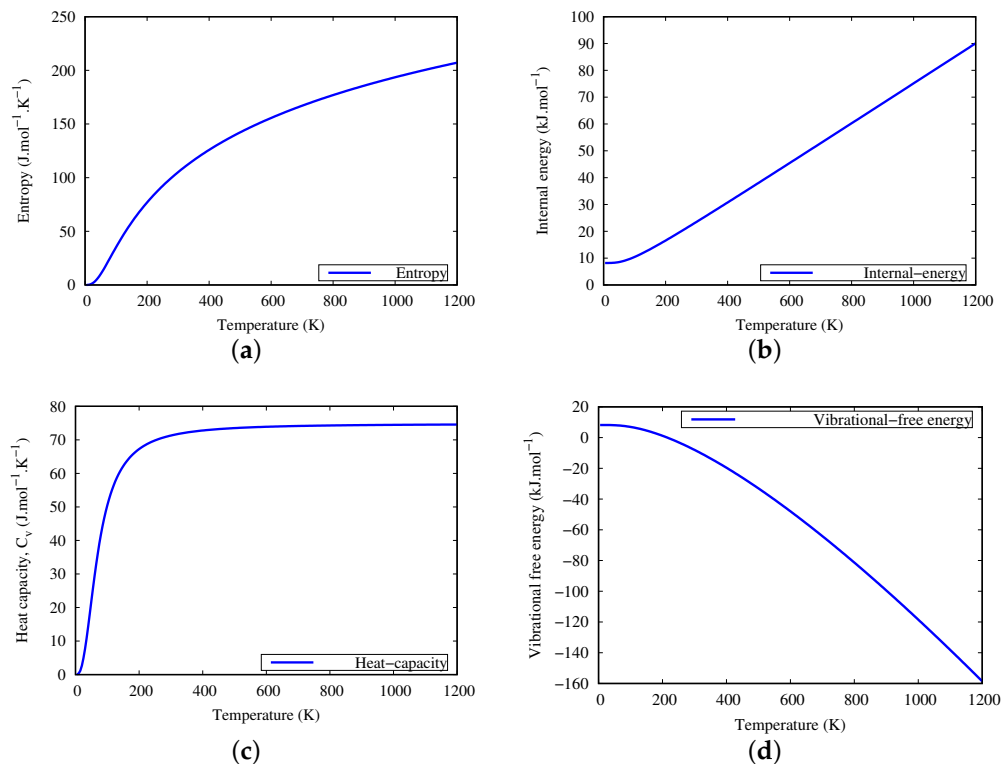


**Figure 3.** Thermodynamic properties of HfIrAs half-Heusler.

### 3.5. Thermoelectric Properties of HfIrAs

The thermoelectric properties were computed using BoltzTraP code [55,56]; this code assumes that the carriers in the narrow energy range near the Fermi level majorly contribute to the transport properties of materials. Therefore it is assumed that the relaxation time for all carriers within this range are constant. The following parameters can be used to evaluate materials’ thermoelectric performance: the Seebeck coefficient, the power factor, and the dimensionless figure of merit. The electrical conductivity of the material slightly decreases with an increase in temperature (see Figure 4a). The Seebeck coefficient as a function of carrier concentration is given in Figure 4b. The maximum Seebeck coefficient obtained in this calculation is  $210 \mu\text{V}/\text{K}$ , a value that is comparable to the Seebeck coefficient of good thermoelectric materials [77]. Therefore, HfIrAs is predicted to be a good thermoelectric candidate. The power factor of the material increases with an increase in temperature (Figure 4c). Its values at 300K, 600K, and 800K are 3.90, 10.28, and 14.85, respectively. The material conversion of thermal energy to electrical energy is favored by the rise in temperature. The dimensionless figure of merit ( $ZT$ ) of HfIrAs at 300 K, 600 K, and 800 K is 0.23, 0.5, and 0.57, respectively (see Figure 4d). The  $ZT$ s obtained in this work are comparable to that of a good thermoelectric candidate from previous similar work [78]. The  $ZT$  of HfIrAs increases with an increase in temperature, and the  $ZT$  of 0.57 shows that HfIrAs is a good thermoelectric material.

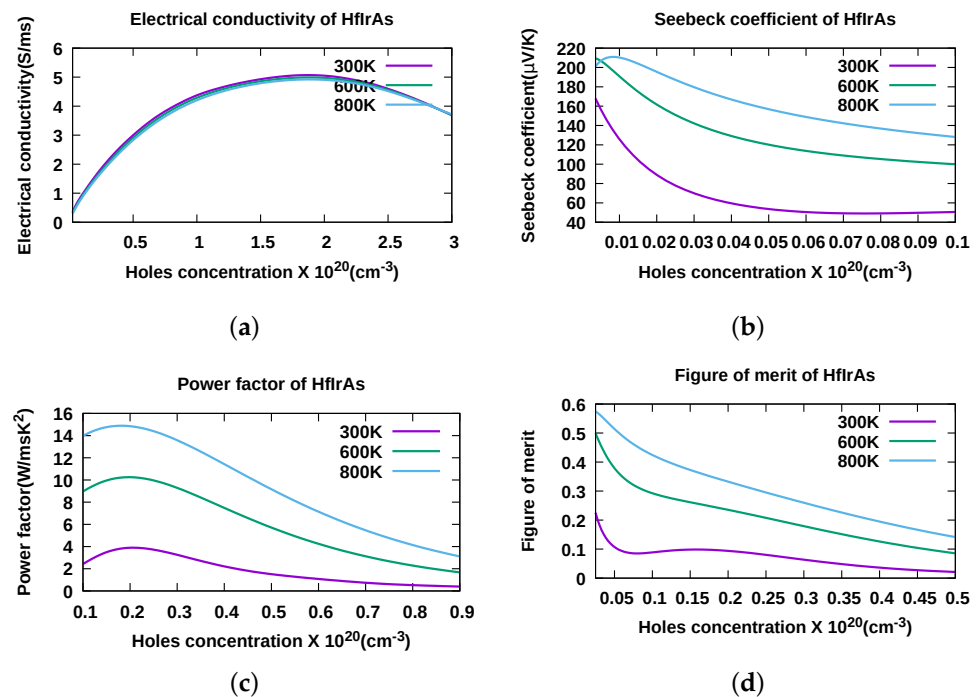


Figure 4. Transport coefficients of HfIrAs half-Heusler.

#### 4. Conclusions

This work calculated the electronic, elastic, optical, and thermoelectric properties of HfIrAs, a semi-metal in the half-Heusler phase. The touching of the bands at  $\gamma$  shows that the compound is a semi-metal. The compound ratio  $B/G$  demonstrates that HfIrAs is ductile and meets mechanical stability conditions. According to the phonon dispersion, the compound is dynamically stable. The specific heat at high temperatures reveals that the material obeys the Dulong–Petit law. The Seebeck coefficient and electronic dimensionless figure of merit show that the material is a good thermoelectric compound.

**Author Contributions:** Conceptualization, G.A.A. and M.K.B.; methodology, G.A.A., M.K.B.; validation, M.K.B., F.A., G.T.S., A.A.M., S.K. and G.A.A.; writing—M.K.B. and G.A.A.; writing—review and editing, M.K.B., A.A.M., S.K. and G.A.A.; supervision, G.A.A. and S.K.; project administration, G.A.A., M.K.B. and S.K.; funding acquisition, S.K. All authors have read and agreed to the published version of the manuscript.

**Funding:** This research received no external funding.

**Data Availability Statement:** Not applicable.

**Acknowledgments:** A. A. Musari appreciates D. P. Joubert and the Centre for High Performance Computing (CHPC), South Africa for granting me access to their HPC cluster for this work. S.K. gratefully acknowledges the Deutsche Forschungsgemeinschaft (DFG, German Research Foundation)—388390466—TRR 247 (2018).

**Conflicts of Interest:** The authors declare no conflict of interest.

#### References

- Kiely, E.; Zwane, R.; Fox, R.; Reilly, A.M.; Guerin, S. Density functional theory predictions of the mechanical properties of crystalline materials. *CrystrEngComm* **2021**, *23*, 5697–5710. [[CrossRef](#)]
- Jain, A.; Shin, Y.; Persson, K.A. Computational predictions of energy materials using density functional theory. *Nat. Rev. Mater.* **2016**, *1*, 15004. [[CrossRef](#)]
- Touzani, R.; Krüger, M. First Principles Density Functional Theory Prediction of the Crystal Structure and the Elastic Properties of Mo<sub>2</sub>ZrB<sub>2</sub> and Mo<sub>2</sub>HfB<sub>2</sub>. *Crystals* **2020**, *10*, 865. [[CrossRef](#)]
- Hasnip, P.J.; Refson, K.; Probert, M.I.J.; Yates, J.R.; Clark, S.J.; Pickard, C.J. Density functional theory in the solid state. *Philos. Trans. R. Soc. A Math. Phys. Eng. Sci.* **2014**, *372*, 20130270. [[CrossRef](#)]

5. Pavarini, E. Solving the strong-correlation problem in materials. *Riv. Nuovo Cim.* **2021**, *44*, 597–640. [[CrossRef](#)]
6. Borlido, P.; Schmidt, J.; Huran, A.W.; Tran, F.; Marques, M.A.L.; Botti, S. Exchange-correlation functionals for band gaps of solids: Benchmark, reparametrization and machine learning. *NPJ Comput. Mater.* **2020**, *6*, 96. [[CrossRef](#)]
7. Lin, L.; Lu, J.; Ying, L. Numerical methods for Kohn–Sham density functional theory. *Acta Numer.* **2019**, *28*, 405–539. [[CrossRef](#)]
8. Woods, N.D.; Payne, M.C.; Hasnip, P.J. Computing the self-consistent field in Kohn–Sham density functional theory. *J. Phys. Condens. Matter* **2019**, *31*, 453001. [[CrossRef](#)]
9. Arbouche, S.C.O.; Amara, K.; Zemouli, M.; Benallou, Y.; Azzaz, Y.; Belgoumène, B.; Elkeurti, M.; Ameri, M. A computational study of the optoelectronic and thermoelectric properties of HfIrX (X = As, Sb and Bi) in the cubic LiAlSi-type structure. *J. Comput. Electron.* **2017**, *16*, 765–775.
10. Gautier, R.; Zhang, X.; Hu, L.; Yu, L.; Lin, Y.; Sunde, T.O.L.; Chon, D.; Poepplmeier, K.R.; Zunger, A. Prediction and accelerated laboratory discovery of previously unknown 18-electron ABX compounds. *Nat. Chem.* **2015**, *7*, 308–316. [[CrossRef](#)]
11. Wang, G.; Wei, J. Topological phase transition in half-Heusler compounds HfIrX (X = As, Sb, Bi). *Comput. Mater. Sci.* **2016**, *124*, 311–315. [[CrossRef](#)]
12. Arikan, N.; Yildiz, G.D.; Yildiz, Y.G.; Iyigör, A. Electronic, Elastic, Vibrational and Thermodynamic Properties of HfIrX (X = As, Sb and Bi) Compounds: Insights from DFT-Based Computer Simulation. *J. Electron. Mater.* **2020**, *49*, 3052–3062. [[CrossRef](#)]
13. Dong, Z.; Luo, J.; Wang, C.; Jiang, Y.; Tan, S.; Zhang, Y.; Grin, Y.; Yu, Z.; Guo, K.; Zhang, J.; et al. Half-Heusler-like compounds with wide continuous compositions and tunable p- to n-type semiconducting thermoelectrics. *Nat. Commun.* **2022**, *13*, 35. [[CrossRef](#)] [[PubMed](#)]
14. Lim, W.Y.S.; Zhang, D.; Duran, S.S.F.; Tan, X.Y.; Tan, C.K.I.; Xu, J.; Suwardi, A. A Systematic Approach for Semiconductor Half-Heusler. *Front. Mater.* **2021**, *8*, 745698. [[CrossRef](#)]
15. Khandy, S.A. Inspecting the electronic structure and thermoelectric power factor of novel p-type half-Heuslers. *Sci. Rep.* **2021**, *11*, 20756. [[CrossRef](#)] [[PubMed](#)]
16. Jaishi, D.R.; Sharma, N.; Karki, B.; Belbase, B.P.; Adhikari, R.P.; Ghimire, M.P. Electronic structure and thermoelectric properties of half-Heusler alloys NiTZ. *AIP Adv.* **2021**, *11*, 025304. [[CrossRef](#)]
17. Zhao, D.; Wang, L.; Bo, L.; Wu, D. Synthesis and Thermoelectric Properties of Ni-Doped ZrCoSb Half-Heusler Compounds. *Metals* **2018**, *8*, 61. [[CrossRef](#)]
18. Yu, J.; Xia, K.; Zhao, X.B.; Zhu, T.-J. High performance p-type half-Heusler thermoelectric materials. *J. Phys. D Appl. Phys.* **2018**, *51*, 113001. [[CrossRef](#)]
19. Kaur, K. TiPdSn: A half Heusler compound with high thermoelectric performance. *Eur. Lett.* **2017**, *117*, 47002. [[CrossRef](#)]
20. Bian, Q. Waste heat: The dominating root cause of current global warming. *Environ. Syst. Res.* **2020**, *9*, 8. [[CrossRef](#)]
21. Poon, S.J. Half-Heusler Compounds: Promising Materials For Mid-To-High Temperature Thermoelectric Conversion. *J. Phys. D Appl. Phys.* **2019**, *52*, 493001. [[CrossRef](#)]
22. Mokhtari, M.; Dahmane, F.; Benabdellah, G.; Zekri, L.; Benalia, S.; Zekri, N. Theoretical study of the structural stability, electronic and magnetic properties of XVsb (X = Fe, Ni, and Co) half-Heusler compounds. *Condens. Matter Phys.* **2018**, *21*, 43705. [[CrossRef](#)]
23. Erkisi, A.; Surucu, G. The investigation of electronic, magnetic, mechanical, and lattice dynamical properties of PdMX (M = Cr, Fe and X = Si and Ge) ferromagnetic half-Heusler metallics: An ab initio study. *Mater. Res. Express* **2017**, *4*, 066504. [[CrossRef](#)]
24. Zhang, R.L.; Damewood, L.; Fong, C.Y.; Yang, L.H.; Peng, R.W.; Felser, C. A half-metallic half-Heusler alloy having the largest atomic-like magnetic moment at optimized lattice constant. *AIP Adv.* **2016**, *6*, 115209. [[CrossRef](#)]
25. Khandy, S.A.; Gupta, D.C. Structural, elastic and magneto-electronic properties of half-metallic BaNpO3 perovskite. *Mater. Chem. Phys.* **2017**, *198*, 380. [[CrossRef](#)]
26. Eliassen, S.N.H.; Katre, A.; Madsen, G.K.H.; Persson, C.; Løvvik, O.M.; Berland, K. Lattice thermal conductivity of  $Ti_x Zr_y Hf_{1-x-y} NiSn$  half-Heusler alloys calculated from first principles: Key role of nature of phonon modes. *Phys. Rev. B* **2017**, *95*, 045202. [[CrossRef](#)]
27. Uto, O.T.; Adebambo, P.O.; Akinlami, J.O.; Kenmoe, S.; Adebayo, G.A. Electronic, Structural, Mechanical, and Thermodynamic Properties of CoYSb (Y = Cr, Mo, W) Half-Heusler Compounds as Potential Spintronic Materials. *Solids* **2022**, *3*, 22–33. [[CrossRef](#)]
28. Khandy, S.A.; Gupta, D.C. DFT investigations on mechanical stability, electronic structure and magnetism in Co<sub>2</sub>TaZ (Z = Al, Ga, In) Heusler alloys. *Semicond. Sci. Technol.* **2017**, *32*, 125019. [[CrossRef](#)]
29. Anand, S.; Xia, K.; Hegde, V.I.; Aydemir, U.; Kocevski, V.; Zhu, T.; Wolverton, C.; Snyder, G.J. A valence balanced rule for discovery of 18-electron half-Heuslers with defects. *Energy Environ. Sci.* **2018**, *11*, 1480. [[CrossRef](#)]
30. Khandy, S.A.; Gupta, D.C. Understanding ferromagnetic phase stability, electronic and transport properties of BaPaO3 and BaNpO3 from Ab-initio calculations. *J. Elect. Mater.* **2017**, *46*, 5531. [[CrossRef](#)]
31. Graf, T.; Felser, C.; Parkin, S.S. Simple rules for the understanding of Heusler compounds. *Prog. Solid State Chem.* **2011**, *39*, 1–50. [[CrossRef](#)]
32. Vikram; Sahni, B.; Barman, C.K.; Alam, A. Accelerated Discovery of New 8-Electron Half-Heusler Compounds as Promising Energy and Topological Quantum Materials. *J. Phys. Chem. C* **2019**, *123*, 7074–7080. [[CrossRef](#)]
33. Shekhar, C.; Kumar, N.; Grinenko, V.; Singh, S.; Sarkar, R.; Luetkens, H.; Wu, S.-C.; Zhang, Y.; Komarek, A.C.; Kampert, E.; et al. Anomalous Hall effect in Weyl semimetal half-Heusler compounds RPtBi (R = Gd and Nd). *Proc. Natl. Acad. Sci. USA* **2018**, *115*, 9140–9144. [[CrossRef](#)] [[PubMed](#)]

34. Zhang, J.; Chen, J.; Li, P.; Zhang, C.; Hou, Z.; Wen, Y.; Zhang, Q.; Wang, W.; Zhang, X. Topological electronic state and anisotropic Fermi surface in half-Heusler GdPtBi. *J. Phys. Condens. Matter* **2020**, *32*, 355707. [[CrossRef](#)] [[PubMed](#)]
35. Nakajima, Y.; Hu, R.; Kirshenbaum, K.; Hughes, A.; Syers, P.; Wang, X.; Wang, K.; Wang, R.; Saha, S.R.; Pratt, D. Topological RPdBi half-Heusler semimetals: A new family of noncentrosymmetric magnetic superconductors. *Sci. Adv.* **2015**, *1*, e1500242. [[CrossRef](#)] [[PubMed](#)]
36. Sandeep; Ghimire, M.P.; Deka, D.; Rai, D.P.; Shankar, A.; Thapa, R.K. Magnetic and electronic properties of half-metallic NiTbSb: A first principles study. *Indian J. Phys.* **2012**, *86*, 301–305. [[CrossRef](#)]
37. Roy, A.; Bennett, J.W.; Rabe, K.M.; Vanderbilt, D. Half-Heusler Semiconductors as Piezoelectrics. *Phys. Rev. Lett.* **2012**, *109*, 037602. [[CrossRef](#)] [[PubMed](#)]
38. Ghimire, M.; Sandeep; Sinha, T.; Thapa, R. First principles study of the electronic and magnetic properties of semi-Heusler alloys NiXSb (X = Ti, V, Cr and Mn). *J. Alloy Compd.* **2011**, *509*, 9742–9752. [[CrossRef](#)]
39. Feng, W.; Xiao, D.; Zhang, Y.; Yao, Y. Half-Heusler topological insulators: A first-principles study with the Tran-Blaha modified Becke-Johnson density functional. *Phys. Rev. B* **2010**, *82*, 235121. [[CrossRef](#)]
40. Chen, L.; Gao, S.; Zeng, X.; Dehkordi, A.M.; Tritt, T.M.; Poon, S.J. Uncovering high thermoelectric figure of merit in (Hf,Zr)NiSn half-Heusler alloys. *Appl. Phys. Lett.* **2015**, *107*, 041902. [[CrossRef](#)]
41. Page, A.; Poudeu, P.F.P.; Uher, C. A first-principles approach to half-Heusler thermoelectrics: Accelerated prediction and understanding of material properties. *J. Mater.* **2016**, *2*, 104–113. [[CrossRef](#)]
42. Burke, K. Perspective on density functional theory. *J. Chem. Phys.* **2012**, *136*, 150901. [[CrossRef](#)] [[PubMed](#)]
43. Cohen, A.J.; Mori-Sanchez, P.; Yang, W. Insights into Current Limitations of Density Functional Theory. *Science* **2008**, *321*, 792–794. [[CrossRef](#)]
44. Kohn, W.; Becke, A.D.; Parr, R.G. Density Functional Theory of Electronic Structure. *J. Phys. Chem.* **1996**, *100*, 12974–12980. [[CrossRef](#)]
45. Runge, E.; Gross, E. Density-Functional Theory for Time-Dependent Systems. *Phys. Rev. Lett.* **1984**, *52*, 997–1000. [[CrossRef](#)]
46. Sham, L.J.; Schlüter, M. Density-Functional Theory of the Energy Gap. *Phys. Rev. Lett.* **1983**, *51*, 1888–1891. [[CrossRef](#)]
47. Karasiev, V.V.; Sjöstrom, T.; Trickey, S.B. Generalized-gradient-approximation noninteracting free-energy functionals for orbital-free density functional calculations. *Phys. Rev. B* **2012**, *86*, 115101. [[CrossRef](#)]
48. Iikura, H.; Tsuneda, T.; Yanai, T.; Hirao, K. A long-range correction scheme for generalized-gradient-approximation exchange functionals. *J. Chem. Phys.* **2001**, *115*, 3540–3544. [[CrossRef](#)]
49. Hua, X.; Chen, X.; Goddard, W.A. Generalized gradient approximation: An improved density-functional theory for accurate orbital eigenvalues. *Phys. Rev. B* **1997**, *55*, 16103–16109. [[CrossRef](#)]
50. Perdew, J.P.; Burke, S.; Ernzerhof, M. Generalized gradient approximation made simple. *Phys. Rev. Lett.* **1996**, *77*, 3865–3868. [[CrossRef](#)]
51. Scandolo, S.; Giannozzi, P.; Cavazzoni, C.; de Gironcoli, S.; Pasquarello, A.; Baroni, S. First-principles codes for computational crystallography in the Quantum-ESPRESSO package. *Z. Krist. Cryst. Mater.* **2005**, *220*, 574–579. [[CrossRef](#)]
52. Giannozzi, P.; Baroni, S.; Bonini, N.; Calandra, M.; Car, R.; Cavazzoni, C.; Ceresoli, D.; Chiarotti, G.L.; Cococcioni, M.; Dabo, I.; et al. QUANTUM ESPRESSO: A modular and open-source software project for quantum simulations of materials. *J. Phys. Condens. Matter* **2009**, *21*, 395502. [[CrossRef](#)] [[PubMed](#)]
53. Giannozzi, P.; Baseggio, O.; Bonfà, P.; Brunato, D.; Car, R.; Carnimeo, I.; Cavazzoni, C.; de Gironcoli, S.; Delugas, P.; Ruffino, F.F.; et al. Quantum ESPRESSO toward the exascale. *J. Chem. Phys.* **2020**, *152*, 154105. [[CrossRef](#)] [[PubMed](#)]
54. Monkhorst, H.J.; Pack, J.D. Special points for Brillouin-zone integrations. *Phys. Rev. B* **1976**, *13*, 5189 [[CrossRef](#)]
55. Madsen, G.K.; Carrete, J.; Verstraete, M.J. BoltzTraP2, a program for interpolating band structures and calculating semi-classical transport coefficients. *Comput. Phys. Commun.* **2018**, *231*, 140–145. [[CrossRef](#)]
56. Madsen, G.K.; Singh, D.J. BoltzTraP. A code for calculating band-structure dependent quantities. *Comput. Phys. Commun.* **2006**, *175*, 67–71. [[CrossRef](#)]
57. Ahmed, R.; Masuri, N.S.; Haq, B.U.; Shaari, A.; AlFaifi, S.; Butt, F.K.; Muhamad, M.N.; Ahmed, M.; Tahir, S.A. Investigations of electronic and thermoelectric properties of half-Heusler alloys XMgN (X = Li, Na, K) by first-principles calculations. *Mater. Des.* **2017**, *136*, 196–203. [[CrossRef](#)]
58. Page, Y.L.; Saxe, P. Symmetry-general least-squares extraction of elastic data for strained materials from ab initio calculations of stress. *Phys. Rev. B* **2002**, *65*, 104104. [[CrossRef](#)]
59. Hill, R. The elastic behaviour of a crystalline aggregate. *Proc. Phys. Soc. Lond.* **1952**, *65*, 349. [[CrossRef](#)]
60. Reuss, A.; *Angew. Z.* Calculation of the centrifugal limit of mixed crystals due to the plasticity condition for single crystals. *Math. Mech.* **1929**, *9*, 49.
61. Born, M.; Huang, K. Dynamical Theory of Crystal Lattices. In *Dynamical Theory of Crystal Lattices*; Oxford Clarendon Press: Oxford, UK, 1956; pp. 120–156.
62. Huntington, H.B. *Solid State Physics, F. Seitz and D. Properties of Engineering Ceramics*; Kriegel, W., Palmour, H., Eds.; Academic Press Inc.: New York, NY, USA, 1958; Volume 7.
63. Voigt, W. *Lehrbuch der Kristallphysik*; B. Teubner: Leipzig, Germany, 1928; p. 739.
64. Yu, W.Y.; Wang, N.; Xiao, X.B.; Tang, B.Y.; Peng, L.M.; Ding, W.J. First-principles investigation of the binary AB<sub>2</sub> type Laves phase in Mg–Al–Ca alloy: Electronic structure and elastic properties. *Solid State Sci.* **2009**, *11*, 1400–1407. [[CrossRef](#)]

65. Li, Y.; Yuan, H.K.; Xia, J.; Zhong, M.M.; Kuang, A.L.; Wang, G.Z.; Zheng, X.R.; Chen, H. First-principles study on structural, electronic, elastic and thermodynamic properties of the full-Heusler alloys Co<sub>2</sub>YZ (Y = Sc, Cr and Z = Al, Ga). *Eur. Phys. J. Appl. Phys.* **2015**, *70*, 31001. [[CrossRef](#)]
66. Chen, X.R.; Zhong, M.M.; Feng, Y.; Zhou, Y.; Yuan, H.K.; Chen, H. Structural, electronic, elastic, and thermodynamic properties of the spin-gapless semiconducting Mn<sub>2</sub>CoAl inverse Heusler alloy under pressure. *Phys. Status Solidi* **2015**, *252*, 2830. [[CrossRef](#)]
67. Huang, H.-M.; Zhang, C.-K.; He, Z.-D.; Zhang, J.; Yang, J.-T.; Luo, S.-J. Electronic and mechanical properties of half-metallic half-Heusler compounds CoCrZ (Z = S, Se, and Te). *Chin. Phys. B* **2018**, *27*, 017103. [[CrossRef](#)]
68. Engineering ToolBox. Metals and Alloys—Bulk Modulus. Available online: [www.engineeringtoolbox.com/bulk-modulus-metals](http://www.engineeringtoolbox.com/bulk-modulus-metals) (accessed on 5 September 2022).
69. Pugh, S.F. XCII. Relations between the elastic moduli and the plastic properties of polycrystalline pure metals. *Philos. Mag.* **1954**, *45*, 823. [[CrossRef](#)]
70. Rogl, G.; Grytsiv, A.; Gürth, M.; Tavassoli, A.; Ebner, C.; Wünschek, A.; Puchegger, S.; Soprunyuk, V.; Schranz, W.; Bauer, E.; et al. Mechanical properties of half-Heusler alloys. *Acta Mater.* **2016**, *107*, 178–195. [[CrossRef](#)]
71. Manna, K.; Sun, Y.; Muechler, L.; Kübler, J.; Felser, C. Heusler, Weyl and Berry. *Nat. Rev. Mater.* **2018**, *3*, 244–256. [[CrossRef](#)]
72. Malakkal, L.; Szpunar, B.; Zuniga, J.C.; Siripurapu, R.K.; Szpunar, J.A. First principles calculation of thermo-mechanical properties of thoria using Quantum ESPRESSO. *Int. J. Comput. Mater. Sci. Eng.* **2016**, *5*, 1650008. [[CrossRef](#)]
73. Rittirum, M.; Yangthaisong, A.; Seetawan, T. Reduced lattice thermal conductivity of Ti-site substituted transition metals Ti<sub>1-x</sub>TMXNiSn: A quasi-harmonic Debye model study. *Chin. J. Phys.* **2019**, *57*, 393–402. [[CrossRef](#)]
74. Baroni, S. Thermodynamics from lattice dynamics with DFT. *EPJ Web Conf.* **2011**, *14*, 02001. [[CrossRef](#)]
75. Baroni, S.; Giannozzi, P.; Isaev, E. Density-Functional Perturbation Theory for Quasi-Harmonic Calculations. *Rev. Miner. Geochem.* **2010**, *71*, 39–57. [[CrossRef](#)]
76. Petit, A.T.; Dulong, P.L. Recherches sur quelques points importants de la theorie de la chaleur. *Ann. Chim. Phys.* **1819**, *10*, 395.
77. Schmitt, J.; Gibbs, Z.M.; Snyder, G.J.; Felser, C. Resolving the true band gap of ZrNiSn half-Heusler thermoelectric materials. *Mater. Horizons* **2014**, *2*, 68–75. [[CrossRef](#)]
78. Rani, B.; Wani, A.F.; Sharopov, U.B.; Patra, L.; Singh, J.; Ali, A.M.; El-Rehim, A.F.A.; Khandy, S.A.; Dhiman, S.; Kaur, K. Electronic Structure-, Phonon Spectrum-, and Effective Mass-Related Thermoelectric Properties of PdXSn (X = Zr, Hf) Half Heuslers. *Molecules* **2022**, *27*, 6567. [[CrossRef](#)] [[PubMed](#)]

**Disclaimer/Publisher’s Note:** The statements, opinions and data contained in all publications are solely those of the individual author(s) and contributor(s) and not of MDPI and/or the editor(s). MDPI and/or the editor(s) disclaim responsibility for any injury to people or property resulting from any ideas, methods, instructions or products referred to in the content.